Turbo-MMC: Minimizing the Submodule Capacitor Size in Modular Multilevel Converters with a Matrix Charge Balancer

Yenan Chen, Youssef Elasser, Ping Wang, Jaeil Baek and Minjie Chen
Princeton University, Princeton, NJ 08540, USA
Email: {yenanc, yelasser, pwang2, jaeil.baek, minjie}@princeton.edu

***Abstract*—This paper presents a Turbo-MMC architecture with a Matrix Charge Balancer (MCB) to minimize the size of the submodule capacitors in modular multilevel converter (MMC) based medium voltage motor drives. The MCB manages the energy in all the submodule capacitors of a standard MMC. It balances the low frequency pulsating power among many MMC submodules and can significantly reduce the submodule capacitor size as well as the voltage ripple. We introduced the operation principles of the Turbo-MMC, and systematically investigated the tradeoffs between the capacitor size reduction and the power conversion stress of the MCB. A distributed phase-shift control strategy was adopted to compress the voltage ripple of the submodule capacitors while maintaining high performance for the MMC. Theoretical analysis and detailed design guidelines for the Turbo-MMC architecture are presented. A scaled-down MMC prototype and a 12-Port MCB have been built and tested to verify the effectiveness of the Turbo-MMC concept.**

***Index Terms*—multilevel modular converter, multiport power converter, power decoupling.**

I. Introduction

Modular multilevel converters (MMCs) offer low device voltage rating, high efficiency and excellent harmonic performance [1]. MMC-derived circuit topologies are applicable to a wide range of power conversion applications including high-voltage direct-current (HVDC) systems and medium voltage (MV) motor drives. The submodule capacitors in an MMC are designed to function as voltage sources and buffer the low frequency pulsating power. The peak to peak amplitude of the ripple power is proportional to the amplitude of the load current, and inversely proportional to the output fundamental frequency [2]. In MV variable speed MMC motor drives, the capacitors suffer the highest stress during start-up and low-speed operation. As shown in Fig. 1, the phase current of a motor drive during start-up is much higher than the nominal operation current of the system [3]. The submodule capacitors have to be sized for the highest current and lowest speed to maintain high power factor, low distortion and safety operation. The submodule capacitors usually contribute more than 50% of system volume and weight.

The low frequency components of pulsating power can be removed by injecting high frequency common mode voltage and circulating current to the phase arms of the MMC [2], [4]. In this way only high frequency pulsating power remains so that the voltage variation of submodule capacitors decreases. However, this method limits the modulation ratio of ac voltage and increases current stress for switches and arm inductors.

978-1-7281-1842-0/19/$31.00 ©2019 IEEE

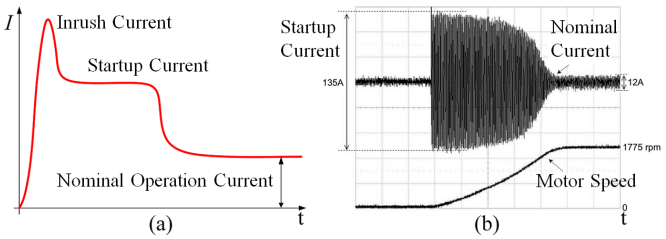

Fig. 1. Typical startup process of a 3-ϕ ac induction motor: (a) phase current amplitude during the startup, (b) phase current waveform and motor speed [3]. The submodule capacitors have the highest operation stress during the startup process. A "Turbo" operation during startup can significantly reduce the design constraints for the submodule capacitor size.

Existing methods for compensating the power flucation in submodule capacitors can be classified into active energy buffers or active energy balance links. In [5], a boost-type active buffer is included in each submodule. The pulsating power in each submodule capacitor is buffered by an active capacitor with large voltage ripple and small capacitance. This method requires a significant number of magnetic components (inductors) and has a theoretical limit in capacitor size reduction. A switched-capacitor-based active energy buffer can eliminate the magnetics as needed in each submodule [6]. The voltage ripple also can be reduced by balancing energy between two submodule capacitors through a dual half-bridge (DHB) converters [7], [8] or among three submodule capacitors through a tri-port half-bridge converter [9], leveraging the naturally balanced pulsating power across submodules and phases. The required magnetic components are also fewer than the standalone active energy buffer.

This paper proposes a Matrix Charge Balancer which links all the submodule capacitors together to compensate the pulsating power and significantly reduce the submodule capacitor size with a "Turbo" operation. Fig. 2 shows the principles of the Turbo-MMC in which all MMC submodule capacitors are connected to a half-bridge unit of the matrix charge balancer which can process the low frequency pulsating power. All the half-bridge units are interconnected by a multiwinding transformer. The MCB only operates with the system for a short period of time during the start-up and heavy load operation of the MMC. It is deactivated during light load situation, which is similar to a turbo engine. A distributed phase-shift (DPS) controller regulates the capacitor voltage of each submodule by changing the phase shift of each half-bridge port. Time domain multiplexing can be applied to

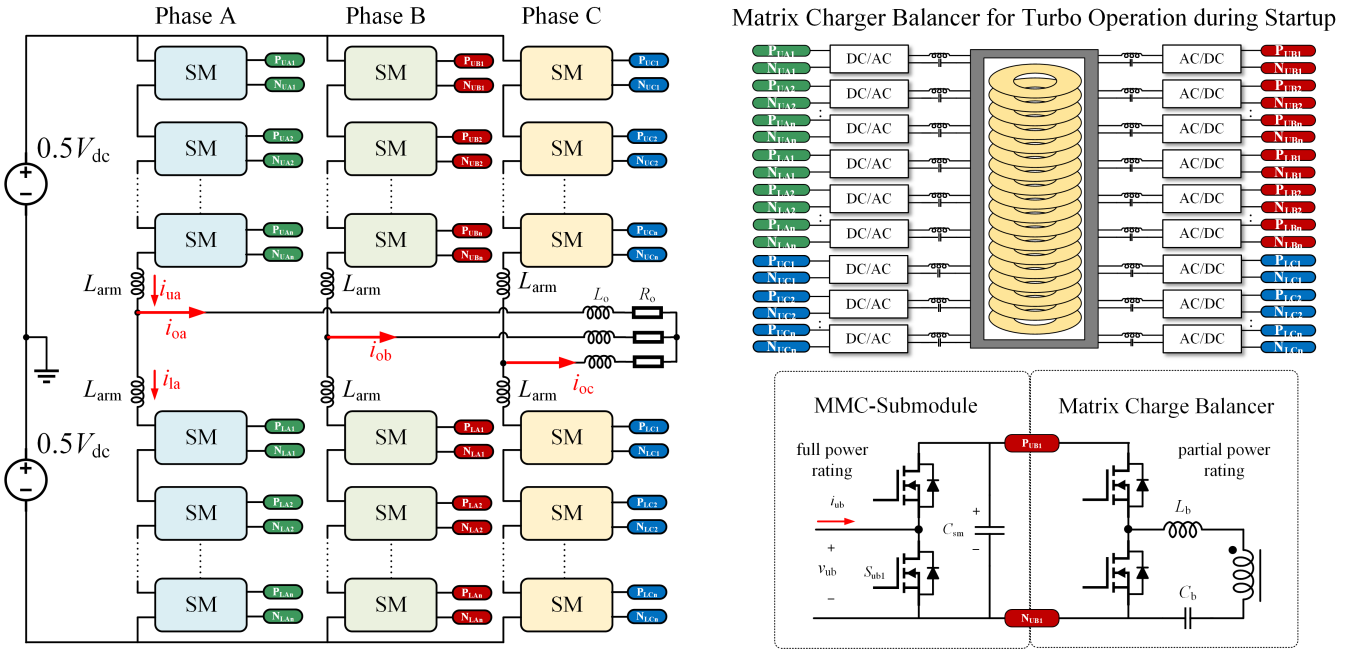

Fig. 2. Block diagram of the 3ϕ Turbo-MMC architecture. All submodule capacitors in the MMC are ac-coupled with a Matrix Charge Balancer (MCB) implemented as a multi-active-bridge converter. The MCB balances the pulsating power in the submodules during the startup process and reduce the energy buffering requirement in the submodule capacitors.

control the power flow. The Turbo-MMC architecture is highly modular and can be implemented in MMC systems with a large number of series stacked submodules.

The remainder of this paper is organized as follows: Section II reviews the principles of pulsating power and voltage ripple in MMCs. Section III presents the principles of the Matrix Charge Balancer together with the MMC systems. Section IV presents the simulation results of the Turbo-MMC. Experimental results of a prototype Turbo-MMC is summarized in Section V. Finally, Section VI concludes the paper.

II. Pulsating Power and Voltage Ripple in MMCs

The 3ϕ MMC topology in Fig. 2 has two arm inductors L_{arm} and $2N$ submodules in each phase arm. The high frequency current and voltage ripples are neglected and switching cycle average is applied to simplify the following analysis. The arm current of Phase A, B, C with balanced load is:

$$i_{ux} = \frac{I_{dc}}{3} + i_{zx} + \frac{i_{ox}}{2},\ i_{lx} = \frac{I_{dc}}{3} + i_{zx} - \frac{i_{ox}}{2}. \quad (1)$$

Here i_{ux} and i_{lx} are the upper arm current and lower arms current respectively. I_d is the dc input current, i_{zx} is the ac circulating current and i_{ox} is the ac output current of the specific phase. With Phase-Shift Carriers SPWM control [1], the input voltage of submudules v_{ux} and v_{lx} are:

$$v_{ux} = \frac{1}{2N}\left(\frac{V_{dc}}{2} - v_{ox}\right),\ v_{lx} = \frac{1}{2N}\left(\frac{V_{dc}}{2} + v_{ox}\right). \quad (2)$$

The ac circulating current is calculated by solving:

$$\frac{\mathrm{d}i_{zx}}{\mathrm{d}t} = \frac{V_{dc}}{2L_{arm}} - \frac{R_{arm}I_{dc}}{3L_{arm}} - \frac{N(v_{ux}+v_{lx})}{2L_{arm}} - \frac{R_{arm}i_{zx}}{L_{arm}}. \quad (3)$$

Here V_{dc} is the dc input voltage and v_{ox} is the phase voltage, R_{arm} is the equivalent resistance of phase arm. Obviously the ac circulating current is caused by the fluctuation of the submodule voltage. The submodule power of upper arm and lower arms are:

$$p_{ux} = v_{ux}i_{ux},\ p_{lx} = v_{lx}i_{lx}. \quad (4)$$

Substituting (1) and (2) into (4) yields:

$$p_{ua}(t) = \frac{V_oI_o}{2N}\Big(\frac{2}{M}\sin(2\pi ft-\varphi) - M\cos\varphi\sin 2\pi ft + \cos(4\pi ft-\varphi)\Big) + \frac{\sqrt{2}V_oi_{za}}{N}\Big(\frac{1}{M} - \sin(2\pi ft-\varphi)\Big), \quad (5)$$

$$p_{la}(t) = \frac{V_oI_o}{2N}\Big(M\cos\varphi\sin 2\pi ft - \frac{2}{M}\sin(2\pi ft-\varphi) + \cos(4\pi ft-\varphi)\Big) + \frac{\sqrt{2}V_oi_{za}}{N}\Big(\frac{1}{M} + \sin(2\pi ft-\varphi)\Big), \quad (6)$$

Here I_o and V_o are the RMS values of the output current and phase voltage, f is the fundamental frequency, M is the voltage amplitude modulation ratio, and φ is the power factor angle. The pulsating power results in voltage ripple on submodule capacitors. For a given submodule capacitance C_{sm}, the peak-to-peak voltage ripple is:

$$\Delta V_{pp} = \frac{N}{2C_{sm}V_{dc}}\int_0^{\frac{1}{f}} |p_{yx}(t)|\ dt. \quad (7)$$

The energy buffered by one submodule capacitor in a fundamental output current cycle is:

$$E_{yx} = \frac{1}{2}\int_0^{\frac{1}{f}} |p_{yx}(t)|\ dt. \quad (8)$$

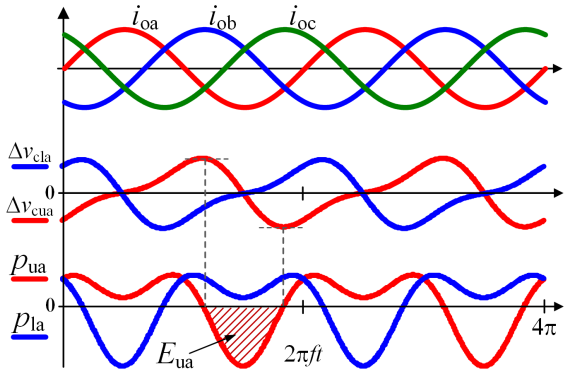

Fig. 3. Voltage ripple and pulsating power of the submodule capacitors in Phase A. i_{oa}, i_{ob} and i_{oc} are the three phase current. Δv_{cla} is the voltage of the submodule capacitor in the lower arm. Δv_{cua} is the voltage of the submodule capacitor in the upper arm. Δp_{ua} is the power processed by the submodule in the lower arm. Δp_{la} is the power processed by the submodule in the upper arm.

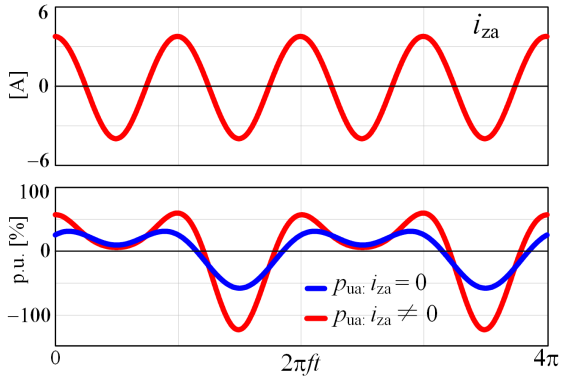

Fig. 4. Calculated ac circulating current and pulsating power of one submodule with different circulating current in Phase A, 1 p.u. = P_o/3. The pulsating power is non-zero even if there is no circulating current. The pulsating power increases as the circulating current increase.

TABLE I
CIRCUIT PARAMETERS OF AN EXAMPLE TURBO-MMC MOTOR DRIVE WITH THE MATRIX CHARGE BALANCER.

V_{dc}	P_o	M	N	f_{mmc}	f_{mab}
700 V	6 kW	0.89	2	10 kHz	100 kHz
L_o	C_{sm}	L_{arm}	R_{arm}	L_b	C_b
2 mH	1 mF	4 mH	50 mΩ	5 μH	0.1 mF

Here y represents the position of phase arm (U: upper arm; L: lower arm). Fig. 3 illustrates the calculated voltage ripple and the pulsating power of upper and lower submodules in one phase arm. With classic SPWM modulation, all the submodules in the same upper arms or lower arms have the same low frequency pulsating power and capacitor voltage ripple. Fig. 3 also indicates that the submodule power on upper arms and lower arms have different polarities in a certain period of time, making it possible to compensate the ripple power between each other and reduce the capacitor size.

With the parameters listed in Table I, the ac circulating current and pulsating power of one submodule is calculated and plotted in Fig. 4. The system is controlled with SPWM without capacitor charge balancing. The frequency of ac circulating current is twice of the fundamental frequency. In this specific case, the peak instantaneous power in each submodule (ac with circulating current) is 125% of the output power of one phase. The total energy buffered in all submodule capacitors is 88% of the overall output energy in this case. If the ac circulating current is zero, 50% of energy needs to be buffered. The ac circulating current in each phase increases the power stress of submodule switches and passive components. It can be reduced by larger submodule capacitors, larger arm inductors and closed-loop control [10].

The purpose of adding a matrix charge balancer to the MMC system is to balance the pulsating power among many submodules, leveraging the fact that the pulsating power in the upper arms and lower arms of the three phases are naturally interleaved. The matrix charge balancer only operate at low frequency and during the startup to significantly reduce the design constraints for the submodule capacitors in a MMC without sacrificing the system efficiency in normal operation.

III. PRINCEPLES OF THE MATRIX CHARGE BALANCER

Fig. 5 illustrates the key operation principles of the Turbo-MMC architecture with a multiport-ac-coupled matrix charge balancer. The Turbo balancer interface with all capacitors, and can freely transfer the pulsating power among multiple capacitors. The Turbo-MMC offers three ways of balancing the pulsating power: 1) balance power vertically among submodules within one phase (red); 2) balance power horizontally among three phases (blue); and 3) balance power as a matrix across submodules and phases (green). The residual pulsating power of the three balancing modes are defined as the average power processed by all involved submodules:

$$
\begin{aligned}
p_v &= \frac{p_{ua}+p_{la}}{2} = \frac{V_o I_o}{2N}\cos(4\pi ft-\varphi) + \frac{\sqrt{2}V_o i_{za}}{NM},\\
p_{h1} &= \sum_{x=a,b,c}\frac{p_{ux}}{3} = \frac{\sqrt{2}V_o}{3N}\left(\frac{\sqrt{3}(i_{zb}-i_{zc})}{2}\cos(2\pi ft-\varphi)\right.\\
&\left. -(i_{za}-\frac{i_{zb}}{2}-\frac{i_{zc}}{2})\sin(2\pi ft-\varphi)+\frac{i_{za}+i_{zb}+i_{zc}}{M}\right),\\
p_{h2} &= \sum_{x=a,b,c}\frac{p_{lx}}{3} = \frac{\sqrt{2}V_o}{3N}\left(-\frac{\sqrt{3}(i_{zb}-i_{zc})}{2}\cos(2\pi ft-\varphi)\right.\\
&\left. +(i_{za}-\frac{i_{zb}}{2}-\frac{i_{zc}}{2})\sin(2\pi ft-\varphi)+\frac{i_{za}+i_{zb}+i_{zc}}{M}\right),\\
p_m &= \sum_{x=a,b,c}\frac{p_{ux}}{6}+\sum_{x=a,b,c}\frac{p_{lx}}{6} = \frac{\sqrt{2}V_o}{3N}\left(\frac{i_{za}+i_{zb}+i_{zc}}{M}\right).
\end{aligned}
\tag{9}
$$

If only vertical balancing strategy is used (energy is transferred from upper arms to lower arms), the residual pulsating power of vertical balancing p_v contains both double-fundamental frequency power fluctuation and ac circulating current. If horizontal balancing is used, the double-fundamental frequency power fluctuation caused by the ac

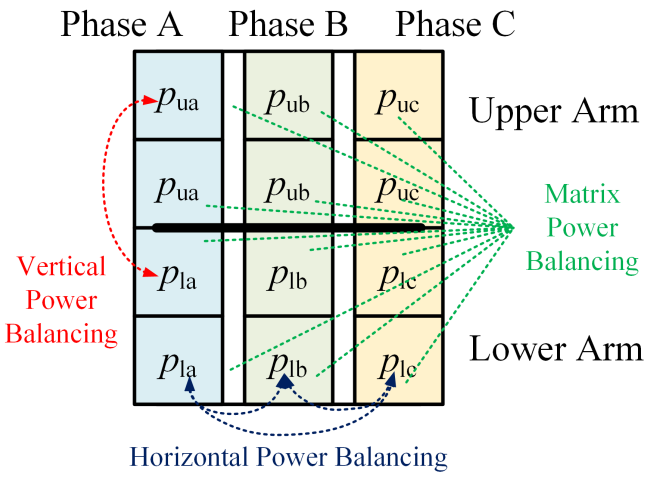

Fig. 5. Three ways of balancing the pulsating power among the submodules.

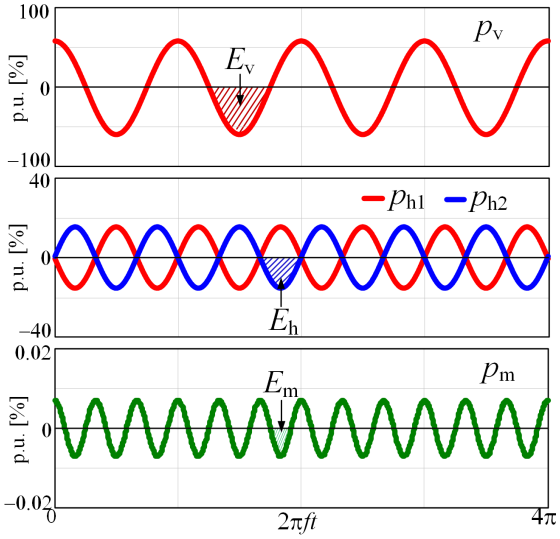

Fig. 6. Percentage of residual unbalanced pulsating power and energy with 1) vertical power balancing (E_v and P_v); 2) horizontal power balancing (E_h and P_h); and 3) matrix power balancing (E_m and P_m), 1 p.u. = $P_o/3$. The voltage ripple can almost be completely eliminated by the matrix power balancing.

output is eliminated. Matrix balancing is a combination of vertical balancing and horizontal balancing, and can fully eliminate the double-fundamental frequency power fluctuation. The ac circulating current can also be reduced by balancing the pulsating power among many submodules.

Fig. 6 compares the remaining pulsating power of one submodule capacitor in an example MMC with 1) vertical power balancing; 2) horizontal power balancing; and 3) matrix power balancing. Matrix power balancing can significantly reduce the peak residual pulsating power. The percentage of energy buffered are calculated based on Eq. (8) and compared in Fig. 7. In the example MMC without pulsating power balancing, over 88% of the energy the MMC processed needs to be buffered by the submodule capacitors. In the example MMC with vertical power balancing, this percentage is reduced to 75%. In the example MMC with horizontal power balancing,

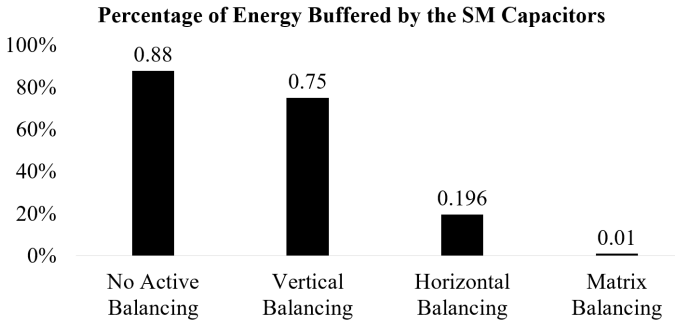

Fig. 7. Percentage of energy buffered by the submodule capacitor with 1) vertical; 2) horizontal; and 3) matrix power balancing. Matrix balancing reduces the percentage of the buffered energy to below 1%. Ideally, no energy needs to be buffered and the submodule capacitors can be fully eliminated.

the percentage of the energy that needs to be buffered is 19.6%. In the example MMC with matrix power balancing, the percentage of the energy that needs to be buffered is less than 1%. Matrix power balancing can almost completely eliminate the pulsating power in the submodule capacitors at the cost of increased power processing stress in the charge balancer. The more energy processed by the matrix charge balancer, the more capacitor size reduction can be achieved.

The smaller submodule capacitor voltage ripple further reduces the ac circulating current in each arm. Balancing the pulsating power not only reduces the submodule capacitor size but also allows smaller arm inductors. However, completely eliminating the submodule capacitor or pursuing zero voltage ripple pushes the power conversion stress to the matrix charge balancer and reduces the system efficiency. The best way to design a Turbo-MMC architecture is to activate the MCB only if needed (i.e., similar to a Turbocharge engine, only operate the matrix charge balancer during the startup when the pulsating power is high), and size the capacitors based on the normal operation to reduce the system volume. Use a MMC with parameters listed in Table I as an example, we investigate the tradeoff between the voltage ripple reduction (which is equivalent to the capacitor size reduction) and the power conversion stress in the Turbo operation with theoretical derivation, SPICE simulations and experiments.

IV. Matrix Charge Balancer

A. Topology and Operation Principles

The matrix charge balancer can be implemented as a multi-active-bridge (MAB) converter as shown in Fig. 8. The MAB converter has many dc-ac inverter units and a multi-winding transformer. By controlling the phase shift of the dc-ac converters, and applying time-domain multiplexing in the dc-ac converters, the matrix charge balancer can route energy from one port to another port, and from multiple input ports to multiple output ports. Other isolated multi-input-multi-output (MIMO) topologies, such as multi-winding flyback and multiport series resonant converter, are also applicable. Implementing the MCB as a MAB converter offers many advantages including high efficiency, high power density, and small magnetic component size. There is only one “dc-ac-dc” power conversion process between two arbitrary ports.

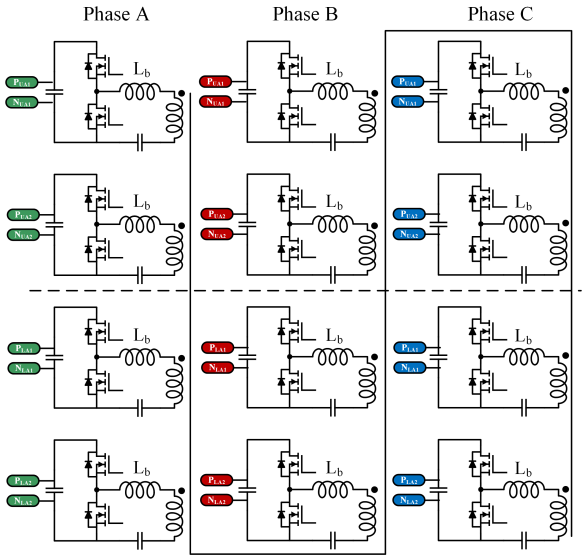

Fig. 8. Matrix charge balancer implemented as a multi-active-bridge converter.

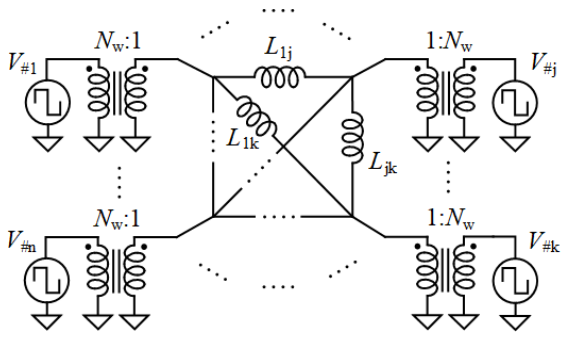

Fig. 9. Simplified ac power flow model of a matrix charge balancer. The multi-winding transformer is modeled as a cantilever model [11] with many inductors directly link from port to port.

B. Power Flow Control Method

The MAB converter delivers power among many submodule capacitors for matrix power balancing. The goal of control the power flow in the MAB converter is to regulate the submodule capacitor voltages. As shown in Fig. 9, the MAB converter with single magnetic core can be modeled as a cantilever model [11] driven by multiple square wave voltage sources. All windings have identical number of turns N_w. In a symmetric multi-winding transformer, the equivalent branch inductance L_{ij} between Port #i and Port #j is [12]:

$$L_{ij} = \frac{6N \cdot L_b}{N_w^2}. \tag{10}$$

Here L_b is the link inductance of each branch. $6N$ is the total number of submodules for a N-level 3ϕ MMC. The average power feed into the multiwinding transformer from Port #i in one switching cycle is:

$$P_i = \frac{V_i}{2\pi f_{mab} N_w^2} \sum_{j \neq i} \frac{V_j}{L_{ij}} (\Phi_j - \Phi_i) \left(1 - \frac{|\Phi_j - \Phi_i|}{\pi}\right). \tag{11}$$

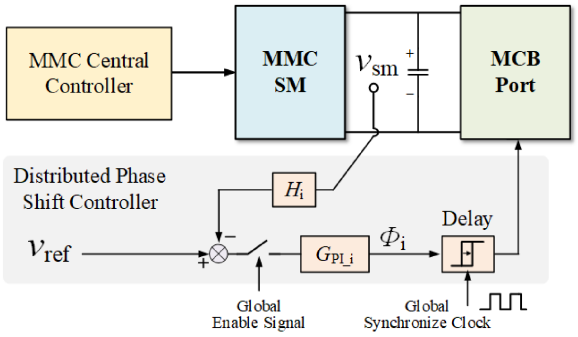

Fig. 10. Distributed phase-shift control for submodule capacitor voltage.

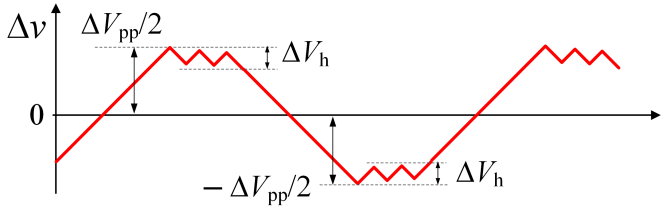

Fig. 11. Hysteresis voltage control strategy for submodule capacitor voltage regulation.

V_i, V_j are the dc voltage of Port #i and Port #j, which is one half of the submodule capacitor voltage $0.5V_{dc}/N$. Φ_i, Φ_j are the phase-shift angles of Port #i and Port #j.

A distributed phase-shift (DPS) controller (as shown in Fig. 11) is designed to control the power flow and regulate the voltage of each submodule capacitor. The DPS block comprises functional blocks such as voltage sensing, error calculation, PI controller and phase-delay module. A global synchronize clock is needed by the DPS block as the absolute phase-shift reference. This DPS controller implementation is highly modular and is applicable to large-scale MMC systems with a large number of submodules.

A hysteresis voltage control strategy is implemented in each DPS controller (Fig. 10). The DPS sets an upper threshold $\Delta V_{pp}/2$, a lower threshold $-\Delta V_{pp}/2$ and a hysteresis ΔV_h for the capacitor voltage, if a capacitor voltage reaches the upper threshold, the MAB converter moves energy away from this capacitor until the voltage ripple drops below $\Delta V_{pp}/2 - \Delta V_h$; if a capacitor voltage reaches the lower threshold, the MAB converter moves energy into this capacitor until the voltage ripple goes above $-\Delta V_{pp}/2 + \Delta V_h$. The matrix power balancing requires exchanging power among all the submodules so that a global enable signal is used to wake up all the half-bridge ports of the MAB converter when any submodule voltage triggers the ripple threshold. Other power flow control strategies, such as ranking the voltage level of all the submodule capacitors and only operate a portion of the ports during a part of the fundamental frequency cycle, are also applicable and are beyond the scope of this paper. Other power flow control methods for MAB converters, such as the Newton-Raphson method based methods as presented in [12], and the time-domain multiplexing method as presented in [13], are also attractive options and are beyond the scope of this paper.

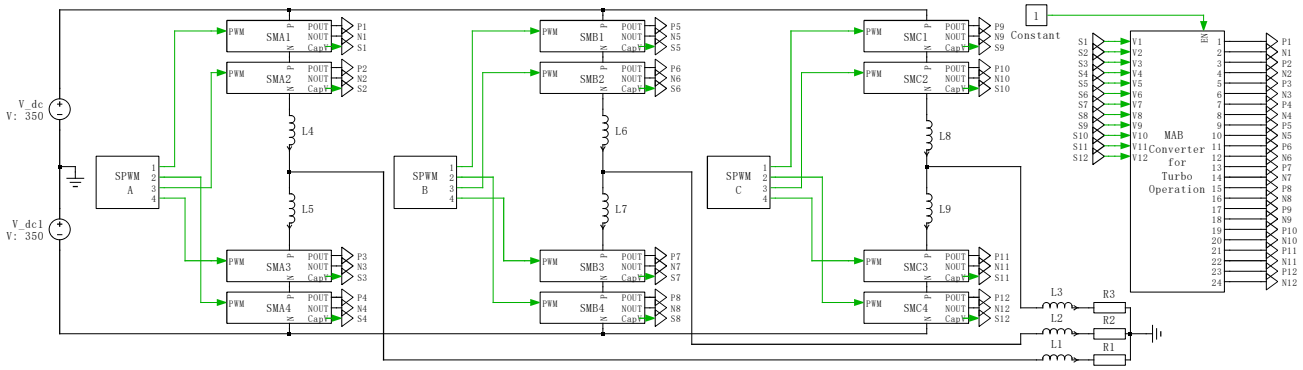

Fig. 12. SPICE simulation platform of a Turbo-MMC comprising a standard 2-level MMC, and a 12-port matrix charge balancer.

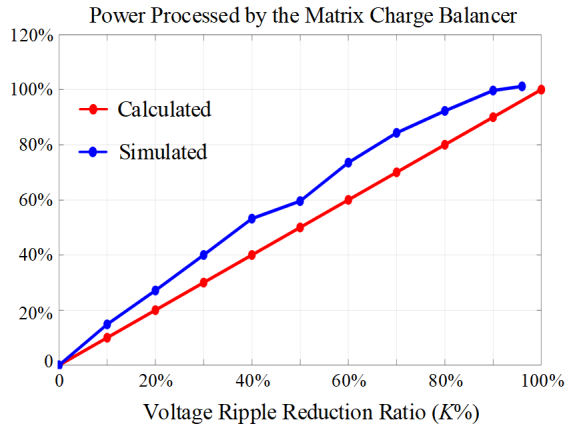

Fig. 13. The voltage ripple compression ratio is linearly proportional to the percentage of power processed by the matrix charge balancer.

C. Turbo Operation and Voltage Ripple Reduction

The pulsating power buffered by the submodule capacitors can almost be completely eliminated by the matrix power balancing, which reduces the device stresses and improves the power quality. On the other hand, processing the pulsating power induces additional loss. For a given submodule design with capacitance C_{sm}, the peak to peak voltage ripple amplitude on the capacitor is a function of the energy buffered by the submodule in Phase x Arm y (E_{yx}):

$$\Delta V_{pp} = \frac{N}{C_{sm} V_{dc}} E_{yx}. \tag{12}$$

V. SPICE Simulations

Fig. 12 shows a SPICE simulation platform for the Turbo-MMC is built in PLECS. Each upper arm and lower arm has two submodules. The carrier frequency of the MMC is 10 kHz and switching frequency of the Turbo balancer is 100 kHz. Other parameters of the MMC system are listed in Table I. Fig. 18 shows the simulation waveforms of voltage ripple on submodule capacitors with different peak to peak ripple threshold. The peak to peak voltage ripple of the submodule capacitors without matrix charge balancing (Turbo mode OFF) is 25 V with a DC offset of 350 V (Fig. 18a). Fig. 18b and

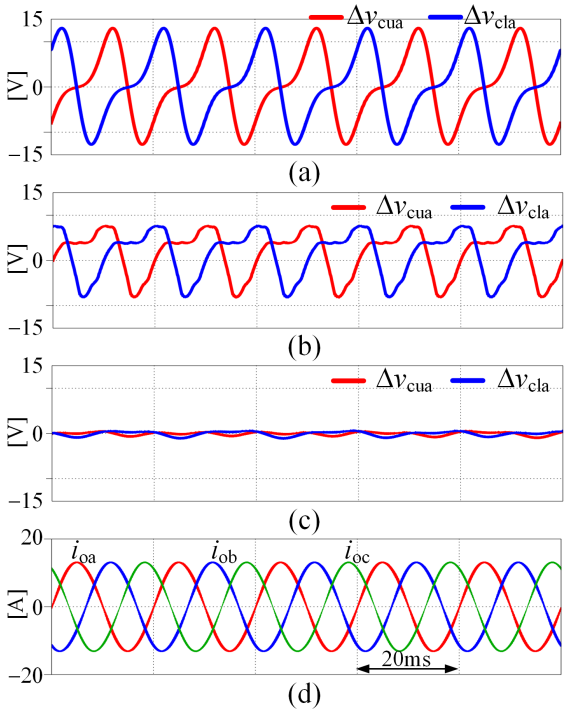

Fig. 14. Simulated waveforms of the submodule capacitor voltage ripple Δv_{cua}, Δv_{cla} in Phase A with C_{sm} = 1mF (a) with Turbo mode OFF, V_{pp} = 25V; (b) with the Turbo mode ON, V_{pp} =12.5V; (c) with the Turbo mode ON, $V_{pp} = 1V$; and (d) three-phase output current.

Fig. 18c show the voltage ripple of the submodule capacitors under Turbo operation. In Fig. 18b, the Turbo operation reduces the peak to peak amplitude of voltage ripple to 12.5 V. In Fig. 18c, the Turbo balancer processes all pulsating power aiming to compress the voltage ripple to zero. The peak to peak voltage ripple is below 1 V (350 V dc offset).

If the MAB converter is controlled in a way to reduce the voltage ripple by $K\%$, the energy that needs to be processed by the MAB converter is $K\%$ of the energy which is processed by this specific submodule. Fig. 13 shows the energy processed by the the MAB converter and the voltage ripple compression ratio for the submodule capacitor. The more power processed by the MAB, the smaller the voltage ripple. The simulation results verified the theoretical analysis.

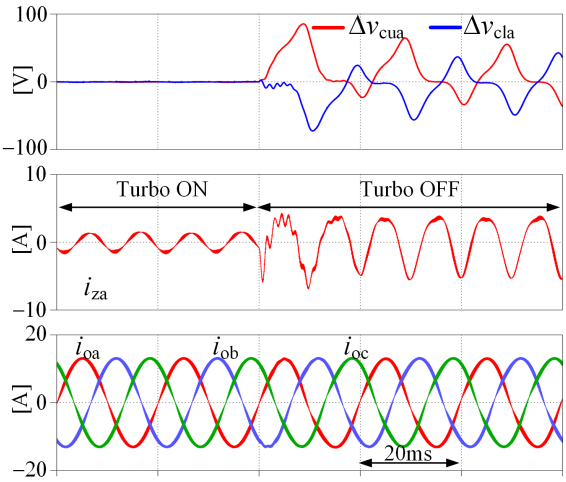

Fig. 15. Simulated waveforms of the submodule capacitor voltage ripple Δv_{cua}, Δv_{cla} and ac circulating current in Phase A with C_{sm}=0.1 mF and L_{arm}=0.4 mH. In Turbo operation, V_{pp} = 1V, the amplitude of circulating current I_{pp} = 2.8A; Without Turbo operation, V_{pp} = 90V, I_{pp} = 8.6A. Turbo-MMC can reduce both voltage ripple and circulating current ripple.

Fig. 15 shows the simulated waveforms of the voltage ripple of submudule capacitors C_{ua} and C_{la}, the ac circulating current of Phase A and the three-phase output current. The simulation is obtained with $C_{sm} = 0.1\ mF$ and $L_{arm} = 0.4\ mH$, which are 10% of the nominal value in in Table I. When the Turbo mode is turned on, the voltage ripple of submodule capacitors is still below 1 V even with much smaller submodule capacitance. After turning off the Turbo operation, the voltage ripple is almost 90 times higher. The amplitude of circulating current also decreases with smaller arm inductors. That can reduce the power loss of the arm inductors and improve power density with small inductor size.

Fig. 16 shows the submodule capacitor voltage of a Turbo-MMC in five operation modes including the transition process. 1) From $0s$ to $0.3s$, the system starts with low frequency (10 Hz) and delivers 1200 W to the load. When starting the motor, low frequency operation causes high fluctuation on the submodule capacitor voltage. The MAB converter is activated to perform Turbo operation from $0s$ to $0.3s$; 2) The Turbo operation is turned OFF while the ac fundamental frequency remains 10 Hz from $0.3s$ to $0.6s$. The capacitor voltage ripple significantly increases; 3) From $0.6s$ to $0.9s$, the system frequency steps up to 50 Hz and the capacitor voltage ripple reduces; 4) From $0.9s$ to $1.2s$, the system output power steps up to full load (6000 W) and the capacitor voltage ripple increases; 5) From $1.2s$ to $1.5s$, the Turbo mode is turned ON, and the capacitor voltage ripple almost reduces to zero.

VI. Experimental Verification

A scaled down Turbo-MMC prototype has been built and tested to verify the matrix pulsating power balancing concept. The prototype includes a low power three-phase MMC converter with 4 modules in each phase and a 12 Port ac-coupled dc-dc converter as the Matrix Charge Balancer. The parameters of the prototype are listed in Table II. The

TABLE II
Parameters of the Turbo-MMC Prototype

Specifications & Symbol	Description
Dc Input Voltage V_{dc}	24 V
Modulation Ratio M	0.89
Fundamental Frequency f	50 Hz
Switching Frequency of MMC f_{mmc}	50 kHz
Submodule Capacitor C_{sm}	330 μF $\times$3
Arm Inductor L_{arm}	7 mH
Output Inductor L_o	0.5 mH
Load Resistor R_o	10 Ω
Port Voltage of MAB V_i	12 V
Switching Frequency of MAB f_{mab}	200 kHz
Blocking Capacitor C_b	0.1 mF
Branch Inductor L_b	0.1 μH
Half-bridge Module	BQ500101 24 V/ 10 A
Transformer Core	EQ30 + PLT30, 3C95
Winding	12$\times$1-Turn, 3$\times$4-Layer PCB

submodule circuits of the MMC converter and the half-bridge ports of MAC converter are implemented with the same half-bridge module. Fig. 17 shows a picture of the prototype. The switching frequency of the MMC is 50 kHz, and the switching frequency of the MAB converter is 200 kHz. Fig. 18 shows the operation waveforms of the prototype with and without the Turbo operation. With Turbo operation, the capacitor voltage ripple is very small. Without the Turbo operation, the voltage ripple increases by almost 8 times. The high voltage ripple also saturated the arm inductors with very high current spikes.

VII. Conclusions

This paper presents a Turbo-MMC architecture to reduce the submodule capacitor size in MMC motor drives. We analyzed the pulsating power and the voltage ripple in MMC submodule capacitors and developed a matrix charge balancer to process the pulsating power. The matrix charge balancer can eliminate the pulsating power in the submodule capacitors and significantly reduce the capacitor size. The Turbo mode should be turned on when the capacitor pulsating power is high (e.g., during system startup, low speed, and heavy load operation) and kept off in nominal operation to maintain high efficiency. The effectiveness of the Turbo-MMC concept is verified by SPICE simulations and experimental results.

Acknowledgment

The authors would like to thank the NSF (#1847365) and the Princeton E-ffiliates program for supporting this work.

References

[1] M. Hagiwara and H. Akagi, "Control and Experiment of Pulsewidth-Modulated Modular Multilevel Converters," *IEEE Transactions on Power Electronics*, vol. 24, no. 7, pp. 1737-1746, July 2009.

[2] A. J. Korn, M. Winkelnkemper and P. Steimer,"Low output frequency operation of the Modular Multi-Level Converter," *2010 IEEE Energy Conversion Congress and Exposition (ECCE)*, Atlanta, GA, 2010, pp. 3993-3997.

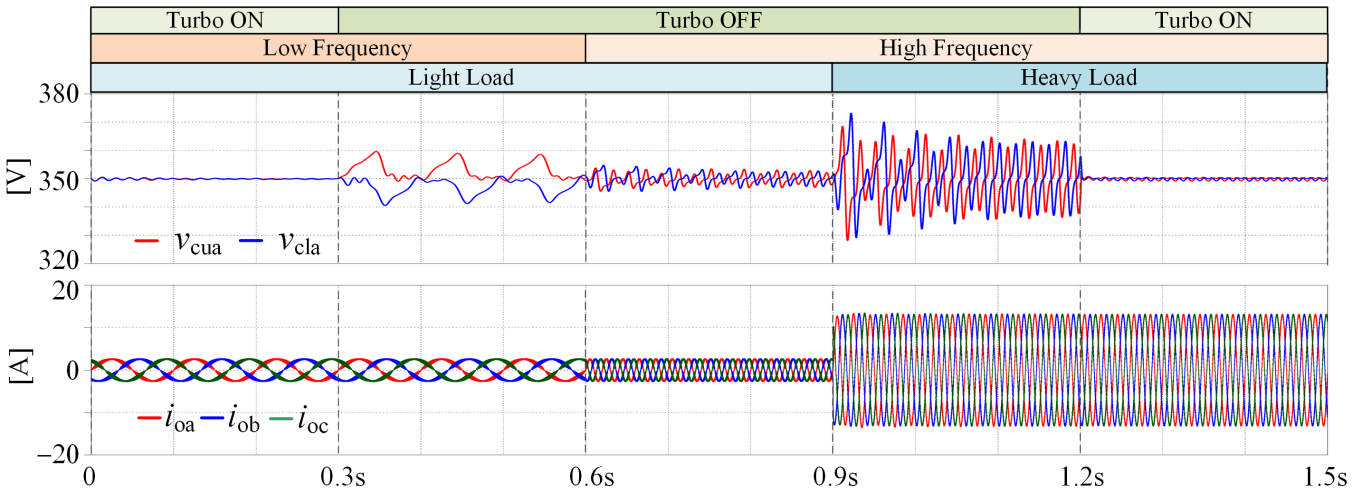

Fig. 16. Simulated capacitor voltage ripple (v_{cua}, v_{cla}) of the Turbo-MMC in five operating modes: (1) 0.0s – 0.3s, low frequency (10 Hz) startup with Turbo mode ON, 20% load (1200 W); (2) 0.3s – 0.6s, light load operation with Turbo mode OFF; (3) 0.6s – 0.9s, output frequency increased to 50Hz with Turbo mode OFF; (4) 0.9s – 1.2s, output load steps up to 100% (6000 W); (5) 1.2s – 1.5s, high frequency heavy load operation with Turbo mode ON.

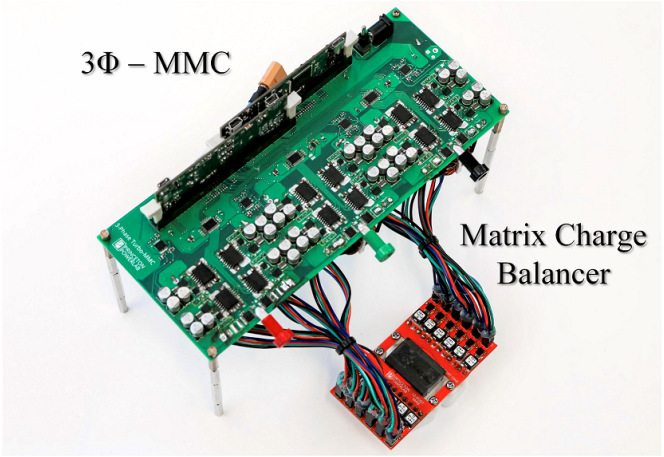

Fig. 17. Picture of the prototype Turbo-MMC with 12 submodules and a 12-port MAB converter.

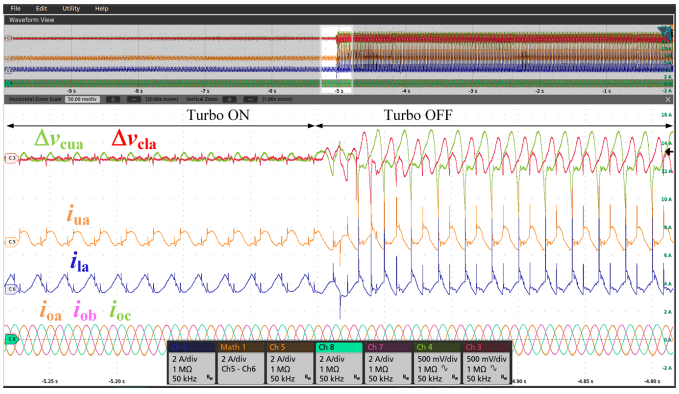

Fig. 18. Measured waveforms of the prototype Turbo-MMC with Output fundamental frequency of 50 Hz. High voltage ripple even causes arm inductor saturation without Turbo operation.

[3] K. Nam, *Motor Control and Electric Vehicle Applications*, Boca Raton, FL, USA: CRC Press, 2010.

[4] M. Hagiwara, I. Hasegawa and H. Akagi, "Start-Up and Low-Speed Operation of an Electric Motor Driven by a Modular Multilevel Cascade Inverter," in *IEEE Transactions on Industry Applications*, vol. 49, no. 4, pp. 1556-1565, July-Aug. 2013.

[5] Z. Kong, X. Huang, Z. Wang, J. Xiong and K. Zhang, "Active Power Decoupling for Submodules of a Modular Multilevel Converter," in *IEEE Transactions on Power Electronics*, vol. 33, no. 1, pp. 125-136, Jan. 2018.

[6] Y. Tang, M. Chen and L. Ran, "A Compact MMC Submodule Structure With Reduced Capacitor Size Using the Stacked Switched Capacitor Architecture," *IEEE Transactions on Power Electronics*, vol. 31, no. 10, pp. 6920-6936, Oct. 2016.

[7] L. He, K. Zhang, J. Xiong, S. Fan, X. Chen and Y. Xue, "New modular multilevel converter with power channels between upper- and lower arms suitable for MV drives," *2015 IEEE Applied Power Electronics Conference and Exposition (APEC)*, Charlotte, NC, 2015, pp. 799-805.

[8] M. S. Diab, A. Massoud, S. Ahmed and B. Williams, "A Modular Multilevel Converter with Ripple-Power Decoupling Channels for Three-Phase MV Adjustable-Speed Drives," in *IEEE Transactions on Power Electronics*, early access.

[9] X. Huang, Z. Wang, Z. Kong, J. Xiong and K. Zhang, "Modular Multilevel Converter With Three-Port Power Channels for Medium-Voltage Drives," in *IEEE Journal of Emerging and Selected Topics in Power Electronics*, vol. 6, no. 3, pp. 1495-1507, Sept. 2018.

[10] Z. Li, P. Wang, Z. Chu, H. Zhu, Y. Luo and Y. Li, "An Inner Current Suppressing Method for Modular Multilevel Converters," in *IEEE Transactions on Power Electronics*, vol. 28, no. 11, pp. 4873-4879, Nov. 2013.

[11] R. W. Erickson and D. Maksimovic, "A multiple-winding magnetics model having directly measurable parameters," *IEEE Power Electronics Specialists Conference*, Fukuoka, 1998, pp. 1472-1478 vol.2.

[12] P. Wang and M. Chen, "Towards Power FPGA: Architecture, Modeling and Control of Multiport Power Converters," *2018 IEEE 19th Workshop on Control and Modeling for Power Electronics (COMPEL)*, Padova, 2018, pp. 1-8.

[13] Y. Chen, P. Wang, H. Li and M. Chen, "Power Flow Control in Multi-Active-Bridge Converters: Theories and Applications," *IEEE Applied Power Electronics Conference and Exposition (APEC)*, Anaheim, CA, USA, 2019, pp. 1500-1507.